386 *Inorg. Chem.* **2010**, *49*, 386–396
DOI: 10.1021/ic901824d

Inorganic Chemistry
Article

Electronic and Magnetic Study of Polycationic Mn_{12} Single-Molecule Magnets with a Ground Spin State S = 11

Juan M. Clemente-Juan,[†,‡] Eugenio Coronado,[*,†] Alicia Forment-Aliaga,[*,†] Alejandro Gaita-Ariño,[†,§] Carlos Giménez-Saiz,[†,‡] Francisco M. Romero,[*,†,‡] W. Wernsdorfer,[⊥] R. Biagi,[#] and V. Corradini[||]

[†]*Instituto de Ciencia Molecular, Universitat de València, Polígono de la Coma, s/n 46980 Paterna, Spain,* [‡]*Fundació General de la Universitat de València,* [§]*Department of Physics and Astronomy and Pacific Institute of Theoretical Physics, University of British Columbia, 6224 Agricultural Road, Vancouver, Canada,* [⊥]*Institut Néel, CNRS & Université J. Fourier, BP 166, 38042, Grenoble, France,* [#]*INFM-CNR S3 National Research Centre and Dipartimento di Fisica, Università di Modena e Reggio Emilia, via G. Campi 213/A, 41100 Modena, Italy, and* [||]*INFM-CNR S3 National Research Centre, via G. Campi 213/A, 41100 Modena, Italy*

Received September 14, 2009

The preparation, magnetic characterization, and X-ray structures of two polycationic Mn_{12} single-molecule magnets $[Mn_{12}O_{12}(bet)_{16}(EtOH)_4](PF_6)_{14}\cdot 4CH_3CN\cdot H_2O$ (**1**) and $[Mn_{12}O_{12}(bet)_{16}(EtOH)_3(H_2O)](PF_6)_{13}(OH)\cdot 6CH_3CN\cdot EtOH\cdot H_2O$ (**2**) (bet = betaine = $(CH_3)_3N^+-CH_2-CO_2^-$) are reported. **1** crystallizes in the centrosymmetric $P2/c$ space group and presents a (0:2:0:2) arrangement of the EtOH molecules in its structure. **2** crystallizes in the noncentrosymmetric $P\bar{4}$ space group with two distinct Mn_{12} polycations, $[Mn_{12}O_{12}(bet)_{16}(EtOH)_2(H_2O)_2]^{14+}$ (2A) and $[Mn_{12}O_{12}(bet)_{16}(EtOH)_4]^{14+}$ (2B) per unit cell. 2A and 2B show a (1:1:1:1) distribution of the coordinated solvent molecules. Interestingly, bond valence sum calculations extracted from X-ray diffraction data indicate the presence of two Mn^{2+} ions in the Mn_{12} core for both **1** and **2**. This finding is confirmed by X-ray absorption spectroscopy (XAS) measurements. A complete magnetic characterization, including subkelvin micro-SQUID magnetometry and inelastic neutron scattering (INS) measurements, permits to extract the parameters of the giant spin Hamiltonian of these polycations. Compared with the archetypal Mn_{12} acetate, an increase in the value of the ground spin state from $S = 10$ to $S = 11$ together with a decrease in the effective energy barrier, is observed for **1** and **2**. Such a result is consistent with the reduction of two Mn^{3+} to the less anisotropic Mn^{2+} ion in the structures.

Introduction

Probably T. Lis never imagined that the molecule he synthesized for the first time in 1980 $[Mn_{12}O_{12}(CH_3CO_2)_{16}(H_2O)_4]$ ($Mn_{12}ac$)[1] would open Pandora's box of molecular magnetism when more than a decade later R. Sessoli and co-workers measured that crystals of this molecule exhibited a superparamagnetic-like behavior characterized by a slow magnetic relaxation below a blocking temperature (T_b).[2] A few years later, quantum tunneling of the magnetization, an effect theoretically predicted by physicists,[3] was observed for first time in these single-molecule magnets (SMMs).[4]

Because the effective energy barrier for spin rotation (and hence T_b) is proportional to the ground spin state and the zero-field splitting of the molecule, an enormous effort has been directed to the synthesis of SMMs with increasing nuclearities and magnetic anisotropies.[5] Still, Mn_{12} derivatives display some of the highest anisotropies and T_b values. Furthermore, they are easy to synthesize and functionalize. In fact, as has been demonstrated in an impressive number of works published by D. N. Hendrickson, G. Christou, and coworkers,[6] $Mn_{12}ac$ has been used as a major source of Mn_{12} molecules prepared by simple ligand exchange reactions. The

*To whom correspondence should be addressed. E-mail: eugenio.coronado@uv.es (E.C.); alicia.forment@uv.es (A.F.-A.).

(1) Lis, T. *Acta Crystallogr., Sect. B* **1980**, *36*, 2042–2046.
(2) Sessoli, R.; Gatteschi, D.; Caneschi, A.; Novak, M. *Nature* **1993**, *365*, 141–143.
(3) (a) Chudnovsky, E. M.; Gunther, L. *Phys. Rev. Lett.* **1988**, *60*, 661–664. (b) Enz, M.; Schilling, R. *J. Phys. C* **1986**, *19*, 1765–1770. (c) van Hemmen, J. L.; Sütö, A. *Physica B+C* **1986**, *141*, 37–75.
(4) (a) Friedman, J. R.; Sarachick, M. P.; Tejada, J.; Ziolo, R. *Phys. Rev. Lett.* **1996**, *76*, 3830–3833. (b) Thomas, L.; Lionti, F.; Ballou, R.; Gatteschi, D.; Sessoli, R.; Barbarca, B. *Nature* **1996**, *383*, 145–147. (c) Hernández, J. M.; Zhang, X. X.; Luis, F.; Bartolomé, J.; Tejada, J.; Ziolo, R. *Europhys. Lett.* **1996**, *35*(4), 301–306.
(5) Sessoli, R. *Inorg. Chim. Acta* **2008**, *361*, 3356–3364.
(6) for example: (a) Sessoli, R.; Tsai, H. L.; Schake, A. R.; Wang, S.; Vicent, J. B.; Folting, K.; Gatteschi, D.; Christou, G.; Hendrickson, D. N. *J. Am. Chem. Soc.* **1993**, *115*, 1804–1816. (b) Rheingold, A.; Christou, G.; Veciana, J.; Hendrickson, D. N. *J. Mater. Chem.* **2002**, *12*, 1152–1161. (c) Eppley, H. J.; Tsuiai, H. L.; de Vries, N.; Folting, K.; Christou, G.; Hendrickson, D. N *J. Am. Chem. Soc.* **1995**, *117*, 301–317. (d) Miyazaki, Y.; Bhattacharjee, A.; Nakano, M.; Saito, K.; Aubin, S. M. J.; Eppley, H. J.; Christou, G.; Hendrickson, D. N.; Sorai, M. *Inorg. Chem.* **2001**, *40*, 6632–6636. (e) Sessoli, R.; Tsai, H. L.; Schake, A. R.; Wang, S.; Vicent, J. B.; Folting, K.; Gatteschi, D.; Christou, G.; Hendrickson, D. N. *J. Am. Chem. Soc.* **1993**, *115*, 1804–1816. (f) Aubin, S. M. J.; Sun, Z.; Guzei, I. A.; Rheingold, A. L.; Christou, G.; Hendrickson, D. N. *Chem. Commun.* **1997**, *19*, 2239–2240.

 Published on Web 10/30/2009

corresponding Mn_{12} derivatives retain their SMM behavior but may have different magnetic properties, better solubility, higher electroaffinity, or higher molecular symmetry, which simplifies the modeling of their magnetic properties.[7] Hence, the Mn_{12} family has been nicknamed the drosophila of single-molecule magnetism.[8]

The preparation of charged derivatives that maintain a SMM behavior opens new gates for the processing of these molecules onto solid surfaces or as multifunctional materials.[9] Electrochemical studies have shown that Mn_{12} complexes are electron acceptors, which are stable upon reduction. Such a feature permits the preparation and crystallization of the $[Mn_{12}]^{n-}$ anions (n = 1, 2, or 3) by chemical reduction of the neutral species.[10] The few magnetic studies reported on these anions indicate that they maintain the SMM behavior, although their ground spin states change, sometimes unpredictably because of the alteration in the competing exchange interactions when the oxidation state of the Mn ions is modified.[8]

However, to date, only two multicationic Mn_{12} derivatives have been reported. The reason for this is that Mn_{12} compounds are poor electron donors and oxidize only under strong conditions to give labile species. The problem can be circumvented through the introduction of positively charged functional groups in the carboxylate ligands of the structure. Using this approach, the polycationic single-molecule magnets $[Mn_{12}O_{12}(Z)_{16}(H_2O)_4](PF_6)_{16}$ (Z = (4-carboxybenzyl)tributylammonium)[11] and $[Mn_{12}O_{12}(bet)_{16}(EtOH)_4](PF_6)_{14}\cdot 4CH_3CN\cdot H_2O$ (**1**) (bet = betaine)[12] were prepared in our group several years ago. Their syntheses are based on the exchange reaction between the acetate bridging ligands in $[Mn_{12}O_{12}(CH_3CO_2)_{16}(H_2O)_4]$ (Mn_{12}ac) and $ZHPF_6$ or $betHPF_6$. An interesting aspect of the betaine-based compound **1** is that X-ray diffraction on single crystals indicates that its manganese core is reduced by two electrons, whereas magnetic measurements are characteristic of a $S = 11$ ground spin state. This is in contrast to previous works on doubly reduced Mn_{12} species, which give invariably $S = 10$ ground spin states.

In this paper, we report on the synthesis and the complete structural and magnetic characterization of two Mn_{12}bet derivatives, namely, compound **1** and the new isomer $[Mn_{12}O_{12}(bet)_{16}(EtOH)_3(H_2O)](PF_6)_{13}(OH)\cdot 6CH_3CN\cdot EtOH\cdot H_2O$ (**2**) obtained also as single crystals through slight changes in the synthetic procedure. Furthermore, the characterization of **1** has been completed with more sophisticated techniques, such as X-ray absorption spectroscopy (XAS), which gives information about the oxidation state of the Mn ions and is an additional proof of the multiply reduced state of the complex, and inelastic neutron scattering (INS) measurements, together with new micro-SQUID measurements of the relaxation of the magnetization at very low temperatures, as independent information sources about its low-energy spin level structure.

Experimental Section

All chemicals and solvents were used as received. $[Mn_{12}O_{12}(CH_3CO_2)_{16}(H_2O)_4]$ (Mn_{12}ac) was prepared by slight modification of the procedure previously reported by T. Lys in 1980.[1] The synthesis of $betHPF_6$ was described in a previous communication.[12]

Preparation of $[Mn_{12}O_{12}(bet)_{16}(EtOH)_4]$ $[PF_6]_{14}\cdot 4CH_3CN$ H_2O (1). Mn_{12}ac (0.125 mmol, 0.25 g) was added to a solution of $betHPF_6$ (2.3 mmol, 0.60 g) in C_6H_5CN (35 mL) and CH_3CN (20 mL). The mixture was stirred overnight, filtered, and the solvent was evaporated under reduced pressure to complete precipitation. The solid was collected by filtration and dissolved in a small amount of CH_3CN. After addition of toluene, the solution was evaporated to dryness to remove the acetic acid as the toluene azeotrope. This stage was repeated twice. The product was then dissolved in C_6H_5CN (35 mL) and CH_3CN (20 mL) and treated again with excess $betHPF_6$. The entire process was repeated. Finally, the product was dissolved in CH_3CN (35 mL). The resulting solution was then filtered and layered with EtOH. Dark brown plates suitable for X-ray crystallography formed after a few days at room temperature. ^{1}H NMR (300.1 MHz, CD_3CN): δ 42−39 (CH_2), 39−33 (CH_2), 30−25 (CH_2), 16.9−15.5 (CH_2), 15.5−14.2 (CH_2), 6.3−4.6 (CH_3), 4.0 (CH_3), 3.01 (CH_3), 2.12 (CH_3), 2.03 (CH_3), 0.80 ppm (CH_3). ^{19}F NMR (282.4 MHz, CD_3CN): δ 68.52 ppm (d, $J(^{19}F, ^{31}P)$ = 709 Hz). ^{31}P NMR (121.5 MHz, CD_3CN): δ −142.20 ppm (m, $J(^{31}P,^{19}F)$ = 709 Hz). IR (KBr, cm^{-1}) 3065 (w), 2967 (w), 1626 (s), 1495 (w), 1436 (m), 1410 (m), 1341 (m), 1240 (w), 967 (w), 910 (w), 837 (s), 725 (w), 619 (w), 558 (m), 461 (w). ESI-MS (CH_3CN, 30 V): m/z 2159 $\{[Mn_{12}O_{12}(bet)_{16}](PF_6)_{11}+1e^{-1}\}^{2+}$; 2086 $\{[Mn_{12}O_{12}(bet)_{16}](PF_6)_{10}+2e^{-1}\}^{2+}$; 2028 $\{[Mn_{12}O_{12}(bet)_{15}](PF_6)_{10}+2e^{-1}\}^{2+}$; 1956 $\{[Mn_{12}O_{12}(bet)_{15}](PF_6)_9+3e^{-1}\}^{2+}$; 1007 $\{[Mn_{12}O_{12}(bet)_{16}](PF_6)_9+1e^{-1}\}^{4+}$, 777 $\{[Mn_{12}O_{12}(bet)_{16}](PF_6)_8+1e^{-1}\}^{5+}$. Elemental anal. Calcd (%) for $[Mn_{12}O_{12}(bet)_{16}](PF_6)_{14}$ (4755.1): C, 20.21; H, 3.73; N, 4.71. Found: C, 19.86; H, 4.26; N, 4.46.

Preparation of $[Mn_{12}O_{12}(bet)_{16}(EtOH)_3(H_2O)]$ $[PF_6]_{13}$ $[OH]\cdot 6CH_3CN$ EtOH H_2O (2). Mn_{12}ac (0.125 mmol, 0.25 g) was added to a solution of $betHPF_6$ (4 mmol, 1.05 g) in CH_3CN (35 mL). The solution was stirred overnight, filtered under a vacuum, and evaporated under reduced pressure to dryness. After addition of toluene, the solution was evaporated to dryness once more in order to eliminate the produced acetic acid as the toluene azeotrope. This stage was repeated twice. A solution of $betHPF_6$ (4 mmol, 1.05 g) in CH_3CN (35 mL) was added to the resulting solid, the mixture was stirred for at least 7 h, and the whole process was repeated. Finally, the product was dissolved in CH_3CN (35 mL), filtered under a vacuum, and layered with absolute ethanol. After a few days, small dark brown prisms suitable for X-ray crystallography were obtained. ^{1}H NMR (400.1 MHz, CD_3CN): δ 44−33 (CH_2), 18−14 (CH_2), 5.44 (CH_3), 4.07 (CH_3), 3.29 (CH_3), 1.82 (CH_3). ^{13}C NMR (75.5 MHz, CD_3CN): δ 208.02, (COOH), 67.90 (CH_2), 30.89 (CH_3);^{19}F NMR (282.4 MHz, CD_3CN): δ = 68.59 (d, $J(^{19}F,^{31}P)$ = 709 Hz). ^{31}P NMR (121.5 MHz, CD_3CN): δ −142.38 (m, $J(^{31}P,^{19}F)$ = 709 Hz). IR (KBr, cm^{-1}): 3065 (w), 2967 (w), 1626 (s), 1495 (w), 1436 (m), 1410 (m), 1341 (m), 1240

(7) (a) Hill, S.; Anderson, N.; Wilson, A.; Takahashi, S.; Petukhov, K.; Chakov, N. E.; Murugesu, M.; North, J. M.; del Barco, E.; Kent, A. D.; Dalal, N. S.; Christou, G. *Polyhedron* **2005**, *24*, 2284–2292. (b) An, J.; Chen, Z. D.; Zhang, X. X.; Raubenheimer, H. G.; Esterhuysen, C.; Gao, S.; Xu, G. X. *J. Chem. Soc., Dalton Trans.* **2001**, *22*, 3352.

(8) Bagai, R.; Christou, G. *Chem. Soc. Rev.* **2009**, *38*, 1011–1026.

(9) (a) Takeda, K.; Awaga, K. *Phys. Rev. B* **1997**, *56*, 14560. (b) Forment-Aliaga, A.; Coronado, E.; Feliz, M.; Gaita-Ariño, A.; Llusar, R.; Romero, F. M. *Inorg. Chem.* **2003**, *42*, 8019–8027. (c) Coronado, E.; Forment-Aliaga, A.; Romero, F. M.; Corradini, V.; Biagi, R.; De Renzi, V.; Gambardella, A.; del Pennino, U. *Inorg. Chem.* **2005**, *44*, 7693–7695. (d) Martínez, R. V.; García, F.; García, R.; Coronado, E.; Forment-Aliaga, A.; Romero, F. M.; Tatay, S. *Adv. Mater.* **2007**, *19*, 291–295.

(10) (a) Eppley, H. J.; Tsai, H. L.; Devries, N.; Folting, K.; Christou, G.; Hendrickson, D. N. *J. Am. Chem. Soc.* **1995**, *117*, 301. (b) Chakov, N. E.; Soler, M.; Wernsdorfer, W.; Abboud, K. A.; Christou, G. *Inorg. Chem.* **2005**, *44*, 5304–5321. (c) Soler, M.; Wernsdorfer, W.; Abboud, K. A.; Huffman, J. C.; Davidson, E. R.; Hendrickson, D. N.; Christou, G. *J. Am. Chem. Soc.* **2003**, *125*, 3576–3588. (d) Bagai, R.; Christou, G. *Inorg. Chem.* **2007**, *46*, 10810–10818.

(11) Coronado, E.; Feliz, M.; Forment-Aliaga, A.; Gómez-García, C. J.; Llusar, R.; Romero, F. M. *Inorg. Chem.* **2001**, *40*, 6084–6085.

(12) Coronado, E.; Forment-Aliaga, A.; Gaita-Ariño, A.; Giménez-Saiz, C.; Romero, F. M.; Wernsdorfer, W. *Angew. Chem., Int. Ed.* **2004**, *43*, 6152–6156.

(w), 967 (w), 910 (w), 837 (s), 725 (w), 619 (w), 558 (m), 461 (w). Elemental anal. Calcd (%) for $[Mn_{12}O_{12}(bet)_{16}(H_2O)](PF_6)_{13}(OH)\cdot H_2O$ (4664.2): C, 20.61; H, 3.91; N, 4.81. Found: C, 19.98; H, 3.53; N, 4.57.

X-ray Data Collection and Structure Refinement. A dark brown platelike single crystal of **1** and a dark brown prismatic single crystal of **2** were used for data collection at 180(2) and 150(2) K respectively, on a Nonius Kappa CCD diffractometer equipped with a graphite monochromated Mo Kα radiation source (λ = 0.71073 Å). The structures were solved by direct methods (SIR97)[13] and refined against F^2 with a full-matrix least-squares algorithm using SHELX-97[14]and the WinGX (1.64) software package.[15] A multiscan absorption correction, based on equivalent reflections was applied to the data of **1** using the program SORTAV.[16] No absorption correction was performed for **2** because of the size of the crystal.

The asymmetric unit of **1** contains one-half of the Mn_{12} cation, which is related to the other half across a 2-fold rotation axis. One of the Mn atoms (Mn6) is coordinated to two EtOH molecules located in axial positions. The carbon atoms of one of these EtOH molecules show an orientational disorder that was modeled with a set of two positions having refined occupancies close to 0.5. These occupancies were fixed to 0.5 in the last cycles of refinement and refined isotropically. The disordered C atoms were presumed to have the same isotropic displacement parameters. Furthermore, C−C and C−O distances were restrained to be the same for both orientations within the same molecule. This kind of disorder in the coordinated ethanol molecule has also been observed in several Mn-Schiff base complexes.[17] A water molecule having an occupancy factor of 0.5 was located near this disordered EtOH. The other EtOH molecule coordinated to Mn6 is not disordered and was refined anisotropically. Nine different hexafluorophosphate anions were located. Three of them lie on special 2-fold positions and one (located on a general position) has a refined occupancy of 0.5, then accounting for the +14 charge of the Mn_{12} complex in **1**. A view of the position of the anions around the Mn_{12}bet cations is shown in Figure S4a of the Supporting Information. The closest distances between anions and polycations are through the F atoms of the PF_6 and H atoms of betaine ligands and range between 2.1 and 2.6 Å. The shortest contacts between polycations are established through H atoms of betaine ligands of Mn_{12}bet neighbors, being ∼2.6 Å; however, the long distances between the magnetic centers make negligible any possible magnetic interaction. Four CH_3CN molecules were also located having refined occupancies of 0.5. Their occupancies were fixed to this value in the last refinement cycles. Geometrical restraints were applied to some of the hexafluorophosphate anions and solvent molecules, which had high anisotropic displacement parameters (ADPs). All non-hydrogen atoms were refined anisotropically with the exception of the disordered molecules having partial occupancies. The position of the H atoms on C atoms were added in calculated positions and refined riding on the corresponding atoms. H atoms on the oxygen atoms of EtOH molecules were refined using the AFIX 147 instruction of SHELX-97. H atoms of the H_2O molecule were placed in theoretical positions using Nardelli's method.[18] These H atoms were included in structure-factor calculations with fixed positional parameters and isotropic displacement parameters of 0.05 Å^2.

The asymmetric unit of **2** contains two quarters of two different Mn_{12} cations (which have been labeled as **2A** and **2B**). In **2A**, one of the octahedral coordination sites of Mn2 is occupied by one EtOH and one H_2O molecule, which show substitutional disorder with occupancies of 0.5. Therefore, **2A** has four Mn ions that complete their octahedral coordination with $2H_2O$ and 2EtOH molecules randomly distributed over the cluster. **2B** is essentially similar, but now substitutional disorder is not present: the four Mn ions (Mn5) complete their octahedral coordination with four ethanol molecules. For convenience, however, an average formula has been considered, giving rise to the value of Z = 2. The carbon atoms of the trimethylammonium groups belonging to the betaine moieties exhibited high and elongated ADPs because of some degree of rotational disorder around the N−CH_2 bond. The asymmetric unit of **2** contains also the following solvent molecules of crystallization: one H_2O molecule, three CH_3CN molecules, and one EtOH molecule (this one having a refined occupancy of 0.5). Seven different hexafluorophosphate anions were also located, one of them on a special position, giving rise to a total of 13 anions per Mn_{12} cluster. Given the cationic charge of the Mn_{12} clusters in **2** (see subsequent structural and physical discussions in the next sections), one more negative charge is required per Mn_{12} cluster and therefore it is assumed that one of the two water molecules found per Mn_{12} cluster is actually a hydroxide anion although the presence of fluoride anions (instead of hydroxide) could not be completely ruled out. Geometrical restraints were applied to some of the hexafluorophosphate anions and solvent molecules having high ADPs. A view of the position of the anions around the Mn_{12}bet cations is shown in Figure S4b in the Supporting Information. The closest distances between anions and polycations are through the F atoms of the PF_6 and H atoms of ethanol and betaine ligands, (2.2−2.5 Å range). The shortest distances between polycations are established through H atoms of betaine ligands of Mn_{12}bet neighbors, being ∼2.2 Å. Despite this, as has been pointed out for **1**, the long distances between the magnetic centers make negligible any possible magnetic interaction. All hydrogen atoms in **2** (with the exception of H atoms of water and hydroxide which were not located) were added in calculated positions and refined riding on the corresponding atoms. All non-hydrogen atoms were refined anisotropically. Crystallographic data for **1** and **2** are summarized in Table 1.

X-ray Absorption Spectroscopy (XAS). Comparative X-ray Absorption (XAS) on thick films of Mn_{12}ac and **1** deposited by drop-casting on a gold substrate were performed at the ESRF ID8 beamline. The thickness of the deposited film was several tens of micrometers. Unpolarized (isotropic) X-ray absorption spectra were taken at 10 K. Special attention was paid to avoid any radiation damaging during measurements. To this end, measurements were performed at reduced power density. These conditions guaranteed no trace of changes in the spectra due to the radiation exposure during the experiment.

Magnetic Measurements. All the magnetic measurements were carried out on polycrystalline samples with a magnetometer (Quantum Design MPMS-XL-5) equipped with a SQUID sensor. The samples were dispersed in grease to avoid torquing of the crystals. The AC measurements were performed in the temperature range 2−8 K at different frequencies with an oscillating magnetic field H = 0.395 mT. The magnetization data were collected in the H = 0−5 T field range at different temperatures between 2 and 5 K. Low-temperature (0.04−7 K) magnetization measurements were performed on single crystals of **1** and **2** using a micro-SQUID apparatus at different sweep rates between 0.1 and 0.001 T s^{-1}.[19] The applied field was parallel to the experimentally observed easy axis of magnetization.

(13) Altomare, A.; Burla, M. C.; Camalli, M.; Cascarano, G.; Giacovazzo, C.; Guagliardi, A.; Moliterni, A. G. G.; Polidori, G.; Spagna, R. *J. Appl. Crystallogr.* **1999**, *32*, 115.

(14) Sheldrick, G. M., *SHELX-97, an Integrated System for Solving and Refining Crystal Structures from Diffraction Data*; University of Göttingen: Göttingen, Germany, 1997.

(15) Farrugia, L. J. *J. Appl. Crystallogr.* **1999**, *32*, 837.

(16) Blessing, R. H. *J. Appl. Crystallogr.* **1997**, *30*, 421–426.

(17) (a) Oki, A. R.; Hodgson, D. J. *Inorg. Chim. Acta* **1990**, *170*, 65–73. (b) Korendovych, I. V.; Rybak-Akimova, E. V. *Acta Crystallogr., Sect. C* **2004**, *60*, 82–84.

(18) Nardelli, M. *J. Appl. Crystallogr.* **1999**, *32*, 563–571.

(19) Wernsdorfer, W. *Adv. Chem. Phys.* **2001**, *118*, 99.

Table 1. Crystal and Structure Refinement Data for Polycationic Mn_{12} Derivatives **1** and **2**

	1	**2**
empirical formula	$C_{96}H_{214}F_{84}Mn_{12}N_{20}O_{49}P_{14}$	$C_{100}H_{223}F_{78}Mn_{12}N_{22}O_{51}P_{13}$
M_w	5121.73	5093.89
T (K)	180(2)	150(2)
λ (Å)	0.71073	0.71073
cryst syst	monoclinic	tetragonal
space group	$P2/c$	$P\bar{4}$
a (Å)	20.7870(4)	23.4751(3)
b (Å)	18.3190(4)	23.4751(3)
c (Å)	31.1280(7)	18.5932(2)
α (deg)	90	90
β (deg)	117.0730(10)	90
γ (deg)	90	90
V(Å^3)	10554.6(4)	10246.3(2)
Z	2	2
ρ_{calcd} (g cm^{-3})	1.612	1.651
μ ($Mo_{K\alpha}$) (mm^{-1})	0.939	0.956
F(000)	5176	5164
2θ range (deg)	3.54−50.74	4.38−52.10
absorption correction (T_{max}/T_{min})	multiscan (0.9626/0.7613)	none
reflns/unique	112612/19136	128590/19829
R_{int}	0.0868	0.1044
params/restraints	1278/89	1314/25
absolute structure parameter		−0.013(18)
reflns [$I > 2\sigma(I)$][i]	$R_1 = 0.0853$, $wR_2 = 0.2284$	$R_1 = 0.0588$, $wR_2 = 0.1369$
final R (all data)	$R_1 = 0.1304$, $wR_2 = 0.2723$	$R_1 = 0.1011$, $wR_2 = 0.1613$
largest diff. peak and hole	1.135 and −1.378 e Å^{-3}	0.750 and −0.529 e Å^{-3}

[i] $R_1 = \Sigma(F_o - F_c)/\Sigma(F_o)$; $wR_2 = [\Sigma[w(F_o^2 - F_c^2)^2]/\Sigma[w(F_o^2)^2]]^{1/2}$.

Inelastic Neutron Scattering (INS). INS spectra with cold neutrons were recorded on the time-of-flight spectrometer IN6 at the Institut Laue-Langevin (ILL) in Grenoble. The measurements were performed on nondeuterated samples of Mn_{12}ac and **1** in a thin aluminum slab-shaped container at 2, 4, and 9 K with an incident wavelength $\lambda = 5.9$ Å. The data processing involved the subtraction of a background spectrum measured on an empty aluminum container of the same size and calibration of the detectors by means of a spectrum of vanadium metal. Conversion of time-of-flight to energy and data reduction were done with the standard program INX at ILL. The spectra were treated using the free programs gawk and gnuplot.

Other Characterization Techniques. IR transmission measurements of pressed KBr pellets were recorded at room temperature with a Nicolet Avatar 320 FTIR spectrophotometer (4000−400 cm^{-1}). Elemental analysis was carried out on samples dried under vacuum in a CE instruments EA 1110 CHNS analyzer. NMR spectra were recorded on a Bruker Avance DRX 300-MHz spectrometer. ESI mass spectra were recorded on a Waters ZQ mass spectrometer using nitrogen as the drying and nebulizing gas. The equipment was calibrated with appropriate standard samples.

Results and Discussion

Synthesis and Crystal Structure. Polycationic Mn_{12} derivatives **1** and **2** were prepared by the well-known procedure of ligand-exchange reaction between Mn_{12}ac and the incoming acid betHPF$_6$. **1** was prepared using an almost stoichiometric betHPF$_6$:Mn_{12}ac ratio in a mixture of acetonitrile and benzonitrile solvents that avoids the complete dissolution of Mn_{12}ac. It is known that small solvent changes in the synthesis or crystallization processes of Mn_{12} derivatives can strongly influence their magnetic properties due to possible changes in the local site-symmetry and environment around the molecules.[20,10c] This prompted us to make slight variations in the synthesis of **1**, in order to obtain new isomers of these unique multicationic Mn_{12} complexes. We found that the use of 100% acetonitrile as solvent, which permits the complete dissolution of the reactants since the beginning, and the introduction of an excess of the incoming bet ligand yields good-quality single crystals of isomer **2**.

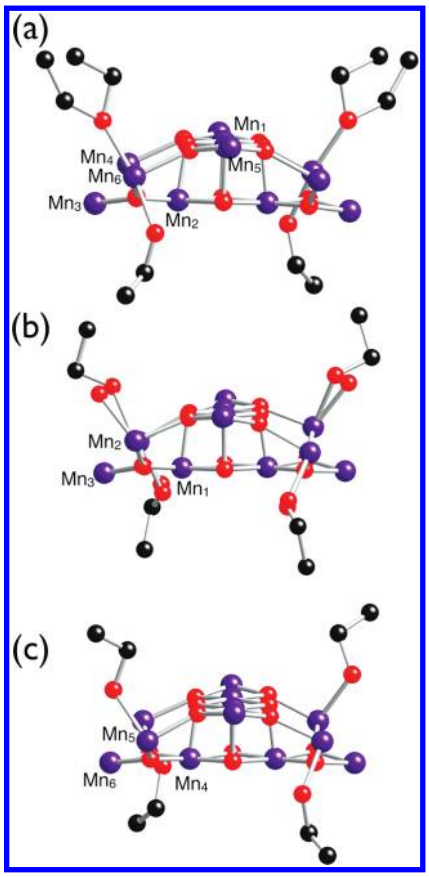

Figure 1. View of the $Mn_{12}O_{12}(EtOH)_{4-n}(H_2O)_n$ moieties of the Mn_{12}bet derivatives (a) **1** ($n = 0$), (b) **2A** ($n = 2$), and (c) **2B** ($n = 0$) showing the EtOH/H_2O molecules coordinated to the partially reduced Mn centers. One coordinated EtOH molecule of **1** shows orientational disorder between two positions. In molecule **2A**, four H_2O molecules with half occupancy disordered over the four terminal ethanol ligand positions are shown. Mn, purple; C, black; and O, red.

The crystal structures of **1** and **2** show $Mn_{12}O_{12}$ moieties similar to those found in other Mn_{12} complexes, showing a central [Mn_4O_4] cubane core surrounded by a non planar [Mn_8O_8] ring held together by μ_3-oxo bridges (Figure S1 in the Supporting Information). Peripheral bridging is ensured by sixteen η^2-μ-betaine ligands, which provide a high positive charge for the polynuclear complexes. In the crystal structure of **1** (space group $P2/c$), there is only one independent Mn_{12} complex that completes its coordination shell with 4 EtOH molecules sitting in the axial positions of two opposite Mn ions, giving rise to a (0:2:0:2) pattern and a local C_2 symmetry for the magnetic cluster (Figure 1a). In contrast, in the prismatic

(20) Soler, M.; Wernsdorfer, W.; Sun, Z. M.; Huffman, J. C.; Hendrickson, D. N.; Christou, G. *Chem. Commun.* **2003**, 2672–2673.

Table 2. Bond Valence Sum Calculations of Mn Oxidation State in the Crystal Structures of **1** and **2**

	Mn^{2+}	Mn^{3+}	Mn^{4+}
		1	
Mn1	4.1066	3.7562	3.9435
Mn2	4.1150	4.7639	3.9546
Mn3	3.2695	2.9905	3.1396
Mn4	2.3139	2.1165	2.2220
Mn5	3.2432	2.9664	3.1143
Mn6	2.3730	2.1705	2.2787
		2A	
Mn1	4.4107	4.0672	3.9910
Mn2(H_2O)	2.5493	2.3508	2.3067
Mn2(EtOH)	2.5571	2.3579	2.3137
Mn3	3.5295	3.2546	3.1936
		2B	
Mn4	4.4429	4.0969	4.0201
Mn5	2.7635	2.5483	2.5006
Mn6	3.4413	3.1733	3.1138

crystals of **2** (space group $P\bar{4}$), two distinct Mn_{12} polycations, **2A** and **2B**, are found per unit cell and both complete their coordination skeleton following a (1:1:1:1) pattern, resulting in a local S_4 symmetry. In **2A**, two H_2O molecules and two EtOH molecules are disordered over the four terminal ligand positions of the polycation (Figure 1b), whereas in **2B** ,there are 4 EtOH molecules with full occupancy (Figure 1c). Both polycations are present in equal amounts in the crystal lattice.

1 and **2** contain, respectively, 14 and 13 hexafluorophosphate anions in the crystal lattice. Considering that complete exchange of the acetate ligands by betaine introduces in the Mn_{12} molecule a positive charge $z = +16$, this finding suggests that **1** and **2** are, respectively, two-electron and three-electron reduced compounds. To check this possibility, we performed bond valence sum (BVS) calculations[21] (Table 2). The structures of the central cubane units compare well with previous results and are characteristic of Mn^{4+} centers. Half of the manganese ions located in the Mn_8 rings (Mn3 and Mn5 in **1**, Mn3 in **2A**, and Mn6 in **2B**, and their symmetry equivalents) are clearly Mn^{3+} and exhibit Jahn−Teller distortion with the anisotropy axes lying almost perpendicular to the mean plane of each $Mn_{12}O_{12}$ fragment.[22] The four remaining coordination sites (Mn4 and Mn6 in **1**, Mn2 in **2A**, and Mn5 in **2B**, and their symmetry equivalents) do not show axial distortion and exhibit longer Mn−O bond lengths, indicating partial reduction to Mn^{2+}. From the BVS analysis, all these Mn atoms are in a +2.5 oxidation state. Therefore, **1** is a two-electron-reduced Mn_{12} salt, where the positive charge of the polynuclear $[Mn_{12}O_{12}(bet)_{16}(EtOH)_4]^{14+}$ complex is exactly compensated by the presence of fourteen hexafluorophosphate anions. Also, **2A** and **2B** are doubly reduced species that can be formulated as $[Mn_{12}O_{12}(bet)_{16}(EtOH)_2(H_2O)_2]^{14+}$ and $[Mn_{12}O_{12}(bet)_{16}(EtOH)_4]^{14+}$, respectively. Here, extra charge compensation may be provided by the presence of one hydroxide or fluoride anion per formula, which can be easily misinterpreted as interstitial water molecules.

Equatorial betaine ligands in **1** and **2** present a propeller-like arrangement. In both structures, molecules with clockwise and anticlockwise arrangements of the betaine ligands around the Mn_8 ring alternate in the crystal lattice to form homochiral layers that lie perpendicular to the main crystallographic axis (Figure 2). In **1**, these layers are related to each other by a center of symmetry, whereas in the noncentrosymmetric structure of **2** they are independent and formed exclusively by **2A** (or **2B**) polycations.

X-ray Absorption Spectroscopy (XAS) Measurements. X-ray absorption spectroscopy (XAS) at the $L_{2,3}$ edges of 3d transition metals is a powerful technique to deeply investigate the electronic structure of metal atoms, particularly their oxidation state, spin state, site symmetry, crystal-field splitting, and degree of covalency.[23] X-ray absorption spectra (Figure 3) were taken at 10 K on thick films of **1** and Mn_{12}ac, deposited by drop-casting on a gold substrate. Attention was paid to avoid any radiation damaging during measurements. The Mn_{12}ac (8 Mn^{3+} and 4 Mn^{4+}) absorption spectrum compares well with literature.[23b] With respect to the acetate derivative, the spectrum of **1** shows a very pronounced contribution around 639 eV, very similar to the characteristic feature of a Mn^{2+} component. The presence of this peak has been already observed on XAS measurements of a one-electron reduced Mn_{12}.[24] This finding evidences the easy reduction of the Mn_{12} derivatives when carboxylates with high electron-withdrawing ability like betaine are introduced in their structure. As has been explained before, this electron-withdrawing ability of the ligands is expected to lower the average oxidation state of two Mn atoms from +3 to +2.[12]

To gather more precise information about the changes induced in the core electronic structure, we subtracted the spectrum of Mn_{12}ac from the spectrum of **1**. In this way, a direct indication of which Mn atoms undergo reduction can be obtained. The difference is reported in Figure 3 and compared with the spectra characteristic of Mn^{2+}, Mn^{3+}, and Mn^{4+}, taken on MnO, Mn_2O_3, and MnO_2 thick films (last two reported upside down for convenience). The positive part fits very well to the Mn^{2+} spectrum, as expected. The comparison of the negative part with the Mn^{3+} and Mn^{4+} spectra indicates that the atoms in the Mn_8 ring (initially Mn^{3+}) are those affected by the reduction process.

A more quantitative analysis can be performed by trying to reproduce the absorption spectrum of **1** starting from that of Mn_{12}ac and adding or subtracting the contributions of the involved oxidation states: the

(21) Brown, I. D.; Altermatt, D. *Acta Crystallogr., Sect. B* **1985**, *41*, 244–247.

(22) Aubin, S. M. J.; Sun, Z.; Eppley, H. J.; Rumberger, E. M.; Guzei, I. A.; Folting, K.; Gantzel, P. K.; Rheingold, A. L.; Christou, G.; Hendrickson, D. N. *Inorg. Chem.* **2001**, *40*, 2127–2146.

(23) (a) Stöhr, J.; Siegmann, H. C. *Magnetism: From Fundamentals to Nanoscale Dynamics*; Springer Series in Solid-State PhysicsSpringer: Berlin, 2006; Vol. *152*. (b) Moroni, R.; Cartier dit Moulin, Ch.; Champion, G.; Arrio, M.-A.; Sainctavit, Ph.; Gatteschi, D. *Phys. Rev. B* **2003**, *68*, 064407. (c) Voss, S.; Fonin, M.; Rüdiger, U.; Burgert, M.; Groth, U.; Dedkov, Yu. S. *Phys. Rev. B* **2007**, *75*, 045102.

(24) Mannini, M.; Sainctavit, P.; Sessoli, R.; Cartier dit Moulin, C.; Pineider, F.; Arrio, M.-A.; Cornia, A.; Gatteschi, D. *Chem.—Eur. J.* **2008**, *14*, 7530–7535.

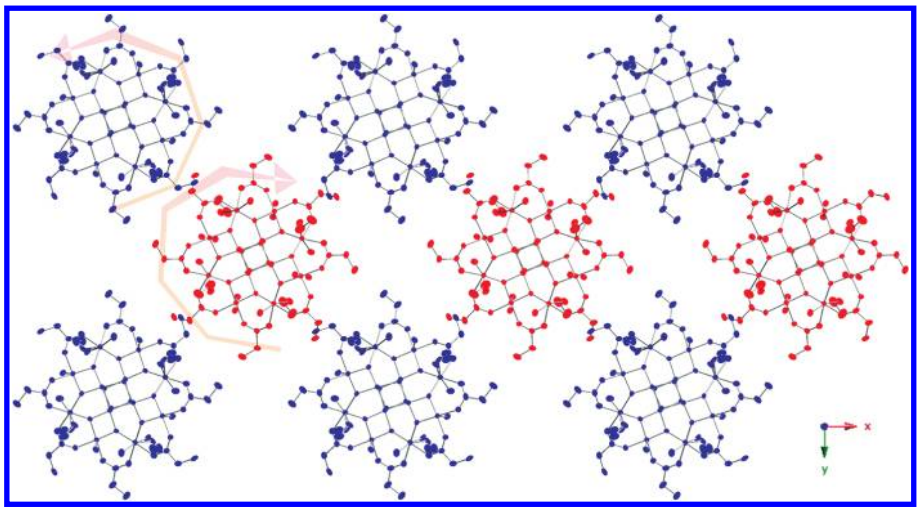

Figure 2. Projection of the crystal structure of **2** onto the *xy* plane showing alternating layers of polycations **2A** (blue) and **2B** (red) with a propeller-like arrangement of the equatorial ligands in counterclockwise and clockwise directions, respectively. Axial carboxylate, methyl groups of betaine ligands, hexafluorophosphate anions, and solvent molecules have been omitted for simplicity.

conversion of n Mn atoms from the oxidation state A to B will be reproduced by subtracting the XAS contribution of n Mn^{A+} and adding the XAS contribution of n Mn^{B+}. This approach, as already pointed out by Mannini et al.,[24] produces better results than building a spectrum of a Mn_{12} compound from a linear combination of its Mn^{X+} components. Actually, since the XAS signal depends on the specific environment, symmetry and crystal field, these components are only representative of the major features of each oxidation state. Their sum cannot reproduce the fine characteristics of a specific compound, especially if it is a complex system like Mn_{12}. For this reason, this analysis is just a semiquantitative[24] approach essentially aimed to extract the main characteristics and does not claim to be rigorous. To correctly perform the calculations outlined above, we need to know the relative contributions of the spectra that we want to combine. Considering that the overall absorption cross-section is proportional to the number of holes in the final shell,[23a] the spectra were normalized so that their areas are proportional to this number. For Mn^{2+}, Mn^{3+}, and Mn^{4+} having 5, 6, and 7 holes (nominally) in the d shell, the areas of the spectra have been normalized to be proportional to 5, 6, and 7, respectively. Correspondingly, the area of the Mn_{12}ac spectrum is taken proportional to $[8 \times 6] + [4 \times 7] = 76$, because it is composed by 8 Mn^{3+} and 4 Mn^{4+}. We found that the spectrum of **1** could be well reproduced by subtracting the contribution of 2.5 ± 0.5 Mn^{3+} ions from the spectrum of Mn_{12}ac and adding that corresponding to the same number of Mn^{2+} ions, i.e., by reducing, in average, about 2.5 Mn atoms from the oxidation state +3 to +2. The comparison of the measured and reconstructed spectrum is shown in Figure 3 and is satisfactory. The introduction of a Mn^{4+} contribution worsens the quality of the fit. These results thus provide the experimental confirmation of the bond valence sum outcome[12] showing a core reduction by two electrons.

Alternating Current (AC) Magnetic Susceptibility Studies. AC magnetic susceptibility measurements were collected on polycrystalline samples of **1** and **2** dispersed on grease in the 2−10 K range at zero DC field and an applied oscillating field of 3.95 G at different frequencies. Table 3 shows a summary of the parameters extracted from the AC magnetic measurements of **1** and **2**. Figure 4a,b shows the temperature dependence of the $\chi'T$ products, where χ' is the real part of the magnetic susceptibility. The plateaus observed at 68−69 emu K mol^{-1} for **1** and 64−65 emu K mol^{-1} for **2** are close to the expected value for an $S = 11$ ground state (66 emu K mol^{-1}) and considerably above the typical values

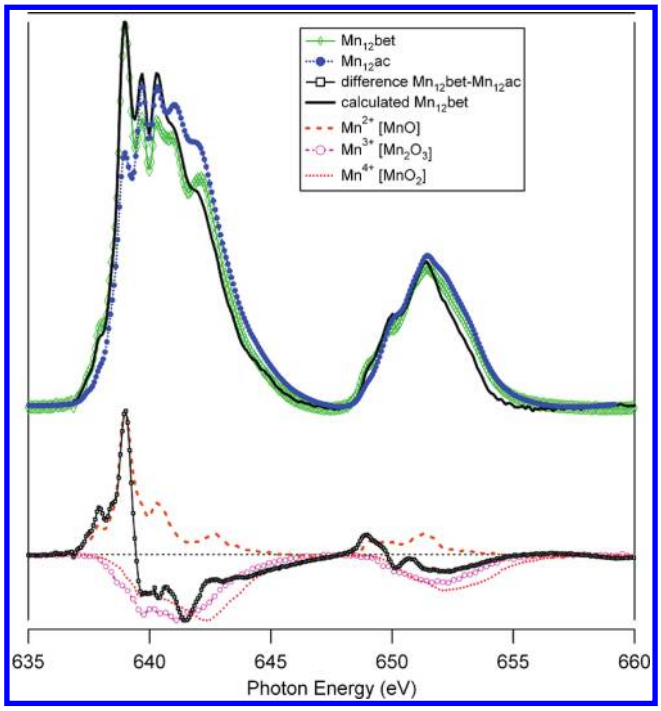

Figure 3. Upper part: Comparison between XAS spectrum of Mn_{12}ac (blue solid circles) and **1** (green diamonds). In black (continuous line) is reported the spectrum of **1** derived from that of Mn_{12}ac by substituting the contribution of 2.5 Mn^{3+} atoms by 2.5 Mn^{2+} atoms. Lower part: difference between the spectra of **1** and Mn_{12}ac (black open squares) compared with the typical XAS spectra of Mn^{2+} (MnO), Mn^{3+} (Mn_2O_3) and Mn^{4+} (MnO_2). For a better comparison of their shape with the difference spectrum, the last two spectra have been reported upside-down and all of them have been normalized to the height of the relevant part (positive or negative) of the difference spectrum.

Table 3. Summary of the Dynamic Magnetic Measurements on **1** and **2** and the Arrhenius Law Parameters Extracted from them; AC Frequencies from 1 to 997 Hz

	1	**2**
$\chi'T$ plateau (emu K mol^{-1})[a]	68−69	64−65
U_{eff}(K)[a]	34.7	33.8
τ_0 (s)[a]	2.1×10^{-10}	4.7×10^{-9}
$U_{eff/1}$ (K)[b]	37	36
$U_{eff/2}$ (K)[b]	19	17
$\tau_{0/1}$ (s)[b]	4×10^{-11}	1×10^{-11}
$\tau_{0/2}$ (s)[b]	3×10^{-5}	3×10^{-4}

[a] Estimated from AC measurement; [b] Estimated from magnetization relaxation measurements on single crystal.

(45−50 emu K mol^{-1}) found in other Mn_{12} compounds. These results confirm those extracted from the DC magnetization fit (see below), avoiding possible complications from the applied dc field and/or low-lying excited states. Frequency-dependent out-of-phase signals (Figures 4c-d), with maxima in the 2−3 K range, were observed for both compounds. χ'' measurements of **1** were performed on wet crystals to be able to obtain well-defined maxima, avoiding the loss of solvent which seems to produce some structural changes and gives rise to a range of Mn_{12} molecular environments, which means different energy barriers and consequently the overlapping of several χ'' peaks. For **2**, well-defined maxima were obtained, even if no special precaution was taken to avoid the loss of solvent. The maxima are relatively broad but this could be explained by the existence of two independent molecules in the crystal plus the disorder in molecules **2A** and **2B**.

From the thermal dependence of these maxima, the effective energy barrier U_{eff} for the reversal of the magnetization and the pre-exponential factor τ_0 can be evaluated using an Arrhenius law (Table 3). Compared with Mn_{12}ac, the lower temperatures ($1 < T < 3.5$ K) at which the χ'' maxima appear, and the lower energy barriers estimated in both compounds (30−35 K instead of 60 K in Mn_{12}Ac), agree with a lower number of anisotropic centers (Mn^{3+}) present in the two-electron-reduced material.

Direct Current (DC) Magnetic Susceptibility Studies. To confirm the spin value of the ground state in compounds **1** and **2** and to determine its anisotropy, we collected DC magnetization data on some crystals of these compounds dispersed on grease, in the $H = 0.1-5$ T field range at different temperatures between $T = 2$ and 5 K (Figure 5). The following fourth-order crystal field Hamiltonian was used as a starting point to fit these data

$$\hat{H} = -gH\mu_B\hat{S} + \sum_{i=0,2} B_2^i O_2^i + \sum_{i=0,4} B_4^i O_4^i \qquad (1)$$

We neglect here the terms of order 6 and higher that are expected to arise from the mixture with excited $S \neq 11$ states[25] because the available experimental data are insufficient to fit such a complex system. Different values of S (9, 10, 11) were tested, fitting the rest of the parameters. In **2**, the Landé factor g rose to unphysical values if left free, so it was fixed to 1.98, a common value in Mn_{12} derivatives. A similar problem was encountered in **1**, but in that case the difference with the expected value lied within the experimental error.

In these conditions, the off-diagonal elements were not found to influence the quality of the fit significantly, so the crystal field Hamiltonian finally used to fit the isofield data is relatively simple

$$\begin{aligned}\hat{H} &= -gH\mu_B\hat{S} + B_2^0\hat{O}_2^0 + B_4^0\hat{O}_4^0 \\ &= -gH\mu_B\hat{S} + D(\hat{S}_z^2 - 1/3\hat{S}(\hat{S}+1)) \\ &+ B_4^0(35\hat{S}_z^4 - 30(\hat{S}(\hat{S}+1) - 25)\hat{S}_z^2 + 3(\hat{S}(\hat{S}+1))^2 \\ &- 6(\hat{S}(\hat{S}+1)))\end{aligned} \qquad (2)$$

where the first term introduces the Zeeman effect, and the second and third terms introduce the quadratic and quartic axial zero-field splitting, respectively. As seen in Figure 5, eq 2 reproduces the magnetization data acceptably. The powder magnetizations have been determined taking into account an integration over all possible orientations of the magnetic field respect to the uniaxial direction of the anisotropy. The best fit values for the different parameters are summarized in Table 4. Still, this procedure has two obvious limitations: first, it cannot account for the dynamic behavior, as it lacks off-diagonal terms that would allow mixing and tunnelling between different states; second, it necessarily results in average parameters for the variety of species derived from structural disorder, positional isomers, and even complexes with different ligands (H_2O vs EtOH).

For both compounds, spin ground states with $S = 11$ were found, which agrees with the value expected from the AC measurements. Moreover, the values of the zero-field splitting parameters ($D = -0.22$ and -0.31 cm^{-1}) estimated by assuming an $S = 11$ ground state match well with the existing data for reduced species.[26] The reduction by two electrons not only substitutes Mn^{3+} for Mn^{2+} − limiting to 6/8 the number of anisotropic ions- but also possibly alters their alignment, further diminishing the total molecular anisotropy. These D values translate into a maximum barrier height U of 31 K for **1** and 47 K for **2** estimated from eq 2 ($E = DM_s^2 + 35B_4^0M_s^4 - 30B_4^0(S(S+1)\text{-}25)M_s^2$). The U-value of **1** is consistent with the effective energy barrier obtained from AC data ($U_{eff} \approx 34$ K). Instead, the U-value derived for **2** from its D parameter is significantly higher than U_{eff}. This mismatch may simply arise from the uncertainty in the determination of D. In fact, from the study of the magnetization vs field measurements in the tunneling regime a more accurate value of D can be extracted (see below). Those measurements are consistent with almost identical D values for **1** and **2** (0.22 and 0.23 cm^{-1}) and therefore with very close energy barriers for both compounds.

Magnetic Studies at Very Low Temperatures. Magnetization measurements were performed at very low temperatures

(25) Wilson, A.; Lawrence, J.; Yang, E.-C.; Nakano, M.; Hendrickson, D. N.; Hill, S. *Phys. Rev. B* **2006**, *74*, R140403.

(26) Typical D values for double reduced Mn_{12} anions found in literature are in the -0.26 to -0.29 cm^{-1} range. (a) Soler, M.; Chandra, S. K.; Ruiz, D.; Huffman, J. C.; Hendrickson, D. N.; Christou, G. *Polyhedron* **2001**, *20*, 1279–1283. (b) See refs 10b, 10c.

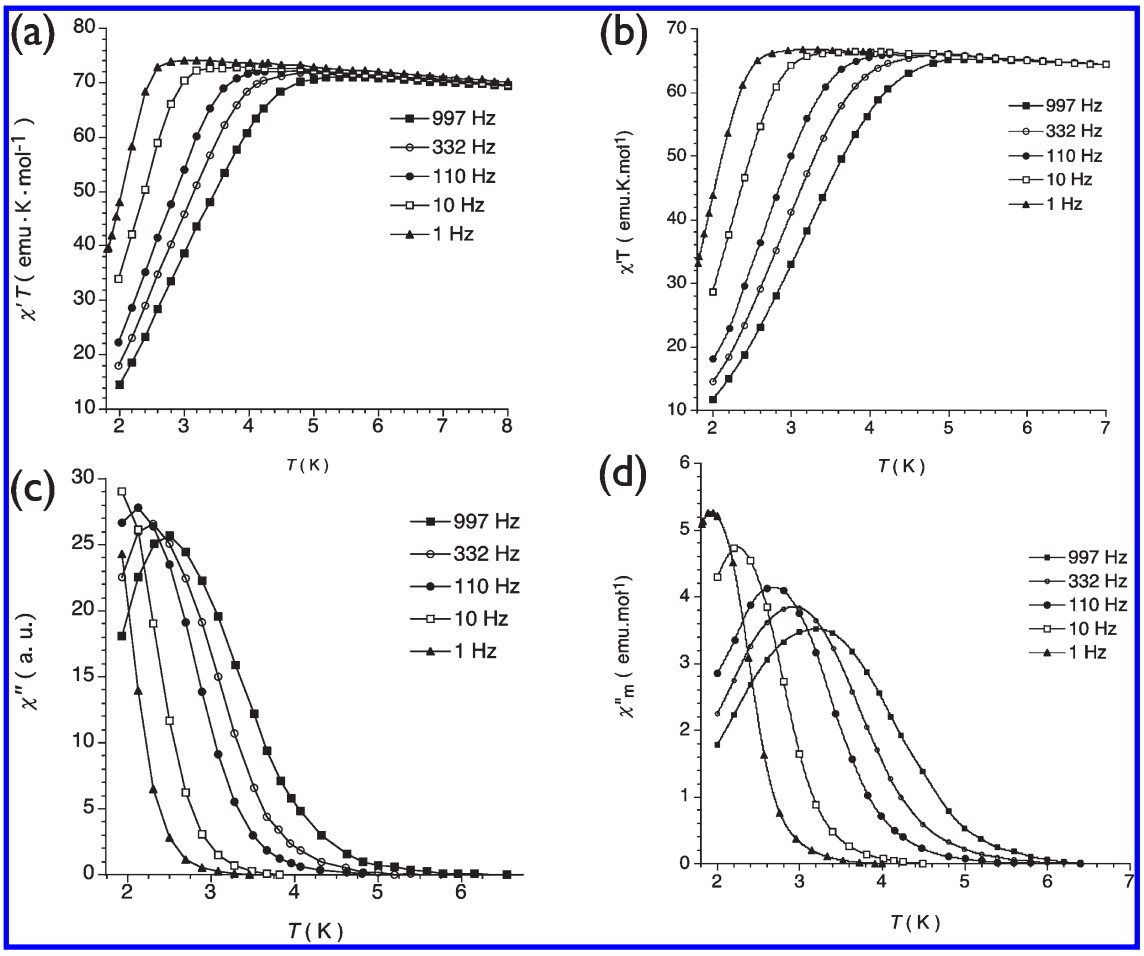

Figure 4. Top: Thermal variation of the $\chi'T$ product of (a) **1** and (b) **2**. Bottom: Temperature dependence of the out-of-phase component of the ac molar magnetic susceptibility of (c) **1** (wet crystals) and (d) **2**. Measurements were performed at different frequencies between 1 and 1000 Hz.

on one single crystal of each compound using a micro-SQUID apparatus. The applied field was set parallel to the experimentally observed easy axis of magnetization. The results of both compounds are very similar. The presence of hysteresis loops in the 1.6−0.04 K range confirms their SMM behavior. These loops are strongly dependent on temperature (Figure 6) and field sweep rate (Figure 7). In contrast with the situation found in most Mn_{12} derivatives, hysteresis was only observed at temperatures below 2 K, a fact that indicates fast relaxation and correlates with the decrease of the effective energy barrier that occurs upon reduction. Quantum tunnelling of the magnetization in the ground state is evidenced by the observation of temperature-independent loops below about 0.3 K that remain strongly dependent on field sweep rate. Quantum steps are observed with a regular[27] spacing $\triangle H = 0.24$ T for both compounds. Hence, as $|D| = \triangle H g \mu_B$, absolute zero-field splitting parameters of 0.23 cm^{-1} for **1** and 0.22 cm^{-1} for **2** are obtained. These values are smaller than those reported for neutral Mn_{12} derivatives. It is worth to remark that the steps smear and become undetectable at high temperatures and/or low magnetic fields. This is probably due to the presence of low-lying excited spin states, although the existence of Mn_{12} molecules with slightly different environments due to partial desolvation and/or solvent disorder could also account for this behavior.

Magnetization relaxation measurements of **1** and **2** were also performed in the micro-SQUID apparatus on oriented single crystals (see Figure S2 in the Supporting Information). Figure 8 is an Arrhenius plot showing the temperature dependence of the magnetization relaxation time τ for both. If the relaxation of the magnetization was thermally activated over a unique energy barrier, τ would follow Arrhenius law and $\ln(\tau)$ vs $1/T$ should give a straight line with a well-defined slope. However, in the case of the two polycationic Mn_{12} derivatives there are three different parts in the Arrhenius plot with three different slopes. At low T, slope is 0 because relaxation takes place by means of quantum tunnelling through the ground state (thermal energy does not suffice to overcome the energy barrier) in a temperature-independent fashion. At temperatures higher than 0.2 K, thermal relaxation takes place and two more slopes can be fitted, presumably showing a distribution of energy barriers, arising either from the different isomers, from low-lying states with $S \neq 11$, or both. This would justify the broad peaks of the AC measurements.

Inelastic Neutron Scattering measurements. Inelastic Neutron Scattering (INS) measurements were performed on crushed single crystals of **1**, at a neutron wavelength $\lambda = 5.9$ Å, at $2\text{ K} < T < 10$ K. INS spectra at 2, 4, and 9 K are displayed in Figure 9, shifted for clarity by 0, 0.25, and

(27) The interval between all steps is not identical as it would be for a simple D system because of the effect of higher-order terms (B_4^0, etc.)

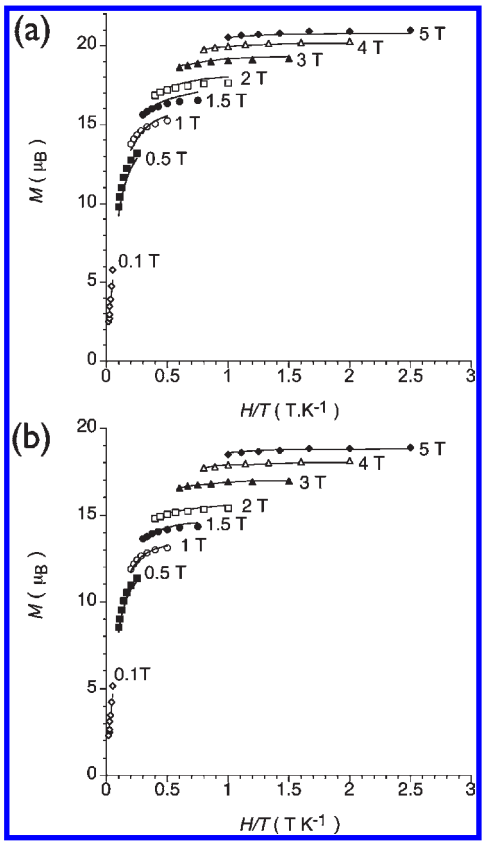

Figure 5. Plots of the magnetization versus H/T for (a) **1** and (b) **2**, at the indicated applied fields. The isofield lines are least-squares fits to the data according with eq 2.

Table 4. Magnetic Parameters Extracted from DC Measurements

	1	**2**
S^a	11	11
g^a	2.05	1.98[b]
D (cm^{-1})[a]	−0.22	−0.31
B_4^0 (cm^{-1})[a]	4.1×10^{-5}	3.9×10^{-5}
$\|D\|$ (cm^{-1})[c]	0.23	0.22

[a] Estimated from the fitting of the isofield measurements. [b] Frozen at this value during the fit, see text. [c] Estimated from magnetization hysteresis loops on single-crystal measurements.

0.50 au of intensity. The very intense peaks located around −0.85 meV and −0.10 meV are experimental artifacts. We focus on the narrow energy window, from −0.7 to −0.2 meV in the neutron energy loss side, which is free of experimental artifacts. At 1.5 K, there are two clear peaks at energies −0.55 and −0.45 meV, and a shoulder at −0.35 meV. Using an arbitrary temperature-independent baseline and fixed widths and positions for the gaussians that correspond to the transitions between spin levels, we find only slight relative changes in intensities on going from 2 to 4 K, as expected for "cold" peaks. Note that the areas of the gaussians are strongly dependent on the detailed shape of the baseline, so they should not be interpreted quantitatively. At 9 K, the spectrum is smeared out.

The neutron energy gain side (see Figure S3 in the Supporting Information) has a wider useful energy window 0.2−1.0 meV, clean of artifacts at low temperature.

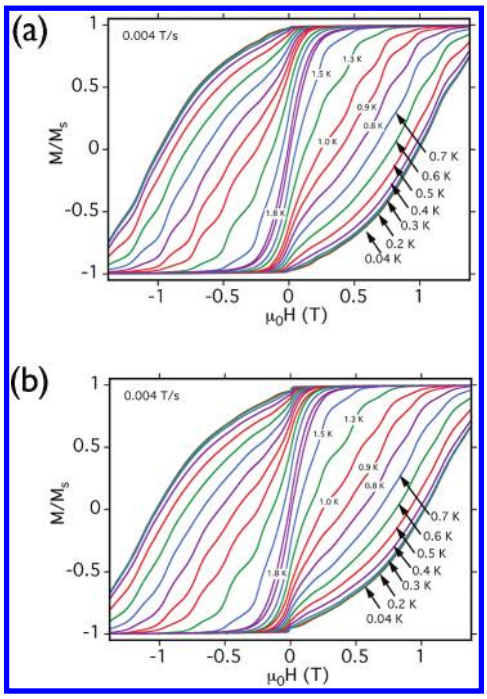

Figure 6. Measurement of reduced magnetization M versus field H applied in the direction of the easy axis of magnetization for compounds (a) **1** and (b) **2** at different temperatures. The sweep rate was 0.004 T/s.

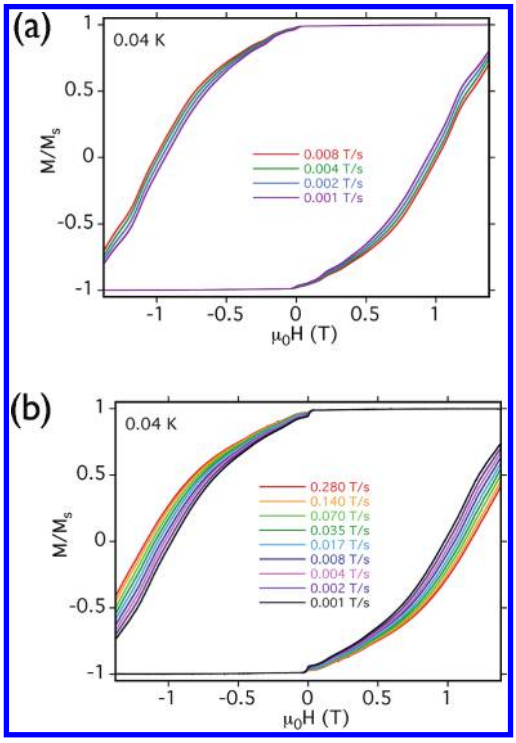

Figure 7. Sweep-rate dependences of the magnetization at 0.04 K of compounds (a) **1** and (b) **2**.

As temperature is raised from 2 to 4 K, then to 9 K, some continuous broad increase in intensity is observed between 0.3 and 0.6 meV, which cannot be easily deconvoluted into individual gaussians. This intensity is probably due to de-excitations corresponding to the excitations observed in the energy loss regime.

The energy range of the transitions is in clear contrast with the usual range found for nonreduced Mn_{12} derivatives,

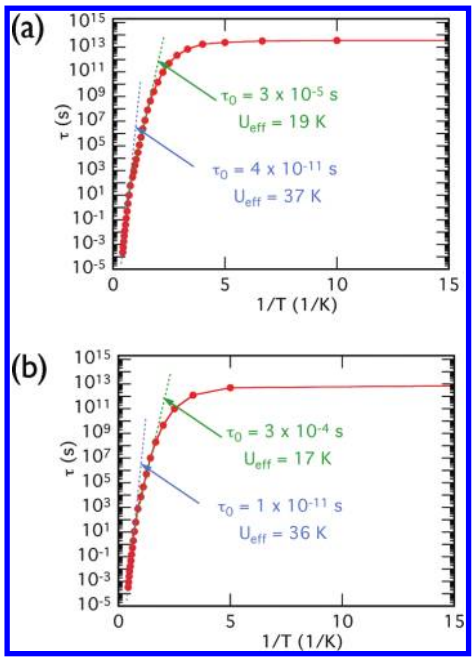

Figure 8. Dependence of the of the relaxation times of the magnetization with the reciprocal temperature (Arrhenius plot) for (a) **1** and (b) **2**.

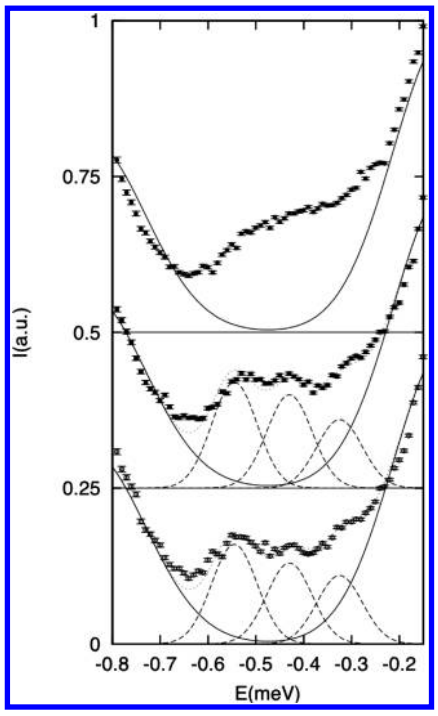

Figure 9. Neutron energy loss side of the inelastic neutron scattering spectra of **1** at different temperatures (9 K full circles, 4 K full square, and 2 K empty circles).

which is approximately double,[28] and is indicative of the strong suppression of the axial zero-field splitting: $D = -0.20\ cm^{-1}$, without higher order terms, corresponds to a $M_S = 11 \rightarrow M_S = 10$ excitation energy of 0.525 meV, and a B_4^0 in the order of 1×10^{-4} to $1 \times 10^{-5} cm^{-1}$ extends this to a range of 0.40−0.66 meV. The low value of D agrees closely with our magnetic study and with previously reported INS data for partially reduced species.[28]

The observation of more than one peak even at temperatures where the Bolzmann distribution of populations ensures the absence of hot transitions is attributed to the presence of isomers, as the 11:9:7 energy ratio precludes the obvious alternative explanation i.e. the presence of extradiagonal terms that mix the states and allow transitions from the ground state to successive excited states. This complexity of our sample prevented us from determining high-order terms, as had been done in previous articles.[29] The positions of the peaks are compatible with isomers with slightly different values of D or B_4^0 in the range of values we estimated from the magnetization data, but the information is insufficient to allow a univocal fit that would have confirmed or refuted the absence of extradiagonal or higher order terms.

Conclusions

In this work, two multicationic Mn_{12} SMMs (**1** and **2**) based on the betaine ligand, obtained under slightly different experimental conditions, have been fully characterized. From a chemical point of view, **1** and **2** differ essentially in the nature and position of the solvent molecules coordinated to the Mn_{12} core. **1** has a local C_2 symmetry and contains four coordinated ethanol molecules in a (0:2:0:2) arrangement, whereas **2** is formed by two distinct Mn_{12} polycations with a (1:1:1:1) distribution of ethanol/water molecules. In spite of the change in symmetry, the differences in the magnetic properties of these complexes are very small. Both behave as SMMs exhibiting very close superparamagnetic energy barriers, $U_{eff} \approx 34$ K, and quantum tunneling effects at very low temperatures.

The introduction of cationic groups in these Mn_{12} complexes seems to enhance their electron acceptor character and spontaneous two-electron reduction is observed. Thus, two anisotropic Mn^{3+} ions have accepted one electron each to become isotropic Mn^{2+} ions, as has been demonstrated in this work by single-crystal X-ray diffraction and XAS measurements. This leads to an increase in the ground spin state of the cluster (from $S = 10$ in Mn_{12}ac to $S = 11$ in **1** and **2**) and to a decrease in the magnetic anisotropy of the cluster (from $D = -0.38\ cm^{-1}$ in Mn_{12}ac to $D \approx -0.22\ cm^{-1}$ in **1** and **2**). The overall effect is a reduction in the energy barrier of the SMM, U_{eff}, which decreases from ca. 60 K in Mn_{12}ac to 34 K in the two polycationic derivatives.

The magnetic characterization of these complexes has been performed by combining AC and DC magnetic measurements with INS data. Quantum tunnelling of the magnetization in these SMMs has been evidenced in single crystals of both derivatives by the observation of temperature-independent hysteresis loops below ca. 0.3 K, and by the presence of quantum steps at low temperatures. Furthermore, magnetization relaxation measurements have shown that in the superparamagnetic regime (i.e., above 0.2 K), both compounds show a distribution of energy barriers arising from the presence of different isomers and/or from low-lying excited states with $S \neq 11$. On the other hand, INS has been a very useful technique to extract independent information about the ground spin level structure, confirming the dramatic quenching of D.

(28) Basler, R.; Sieber, A.; Chaboussant, G.; Güdel, H. U.; Chakov, N. E.; Soler, M.; Christou, G.; Desmedt, A.; Lechner, L. *Inorg. Chem.* **2005**, *44*, 649–653.
(29) Bircher, R.; Chaboussant, G.; Sieber, A.; Güdel, H. U.; Mutka, H. *Phys. Rev. B* **2008**, *70*, 212413.

Given the cationic character of these derivatives and their robustness as SMMs, these molecules are very suitable to be processed taking advantage of the electrostatic interactions established with appropriate counterions. Such features have already been exploited to deposit these cations on functionalized gold surfaces[9c] and on patterned Si surfaces.[9d]

Acknowledgment. Financial support from the European Union (NoE MAGMANet, STEP Project MolSpinQIP and ERC Advanced Grants SPINMOL and MolNanoSpin 226558), the Spanish Ministerio de Ciencia e Innovación (Project Consolider-Ingenio in Molecular Nanoscience, CSD2007-00010, and Projects MAT2007-61584 and CTQ-2008-06720-C02-01/BQU), and the Agence Nationale de la Recherche (MolNanoSpin ANR-08-NANO-002) the Generalitat Valenciana (PROMETEO Program) are gratefully acknowledged. The authors also thank S. Benmansour for her technical support, the European Synchrotron Radiation Facility for provision of synchrotron X-ray radiation facilities, Dr. J. C Cezar for assistance in using beamline ID8, the Institut Laue-Langevin for neutron radiation facilities, and Hannu Muttka for assistance in the ILL installations. A.F.-A. thanks the Spanish Ministerio de Ciencia e Innovación for a Juan de la Cierva contract, and A.G.A. thanks the European Union for a FP7-PEOPLE-2007-4-1-IOF contract.

Supporting Information Available: Figure S1: ORTEP view of polycations **1**, **2A**, and **2B**. Figure S2: Measurement of the relaxation of the reduced magnetization *M* for compound (a) **1** and (b) **2** at different temperatures. Figure S3: Neutron energy gain side of the inelastic neutron scattering spectra of compound **1** at different temperatures. Figure S4: View of the anions in the solid for compound **1** and **2** (PDF). This material is available free of charge via the Internet at http://pubs.acs.org.